Analyzing Uncertainty in Microplastic Detection: A Comprehensive CT Scan and Neural Network Approach

Analyzing Uncertainty in Microplastic Detection: A Comprehensive CT Scan and Neural Network Approach

1st Alessia Caputo
Dept. of Ind. Eng. and Math. Sciences
Polytechnic Univ. of Marche
Ancona, Italia
a.caputo@pm.univpm.it

2nd Pierluigi Strafella
Dept. of Ind. Eng. and Math. Sciences
Polytechnic Univ. of Marche
Ancona, Italia
IRBIM, CNR, Ancona, Italy
p.strafella@pm.univpm.it

3rd Paolo Castellini
Dept. of Ind. Eng. and Math. Sciences
Polytechnic Univ. of Marche
Ancona, Italia
p.castellini@staff.univpm.it

***Abstract*—Microplastics (MPs), smaller than 5 mm and often invisible to the naked eye, represent a significant threat to marine ecosystems and human health. Traditional methods for detecting MPs often lack efficiency and may compromise sample integrity. In this study, a novel non-destructive methodology for detecting MPs in fish samples is proposed, utilizing computed tomography (CT) scanning and neural networks (NN). Leveraging recent advancements in uncertainty analysis, the reliability of the innovative approach and its application to fish sample analysis is assessed. Sources of uncertainty originating from both tomographic imaging and NN processing are identified, addressing issues such as false positives/negatives and uncertainties in measured parameters such as particle position, size, and material. Through post-processing techniques and calibration procedures, uncertainties are mitigated, providing insights into epistemic and stochastic uncertainties inherent in the methodology. Our findings demonstrate that the calibration system used in conjunction with tomographic imaging shows good linearity, with a standard deviation of 0.029 kg/m^3. Despite inherent noise in the images causing variability in gray levels, the range of variability for the plastics of interest was narrower than the uncertainty of the calibration curve. This indicates that while the calibration was accurate, the inherent noise still posed challenges for precise material classification.This comprehensive analysis enhances the reliability and accuracy of MPs detection in fish samples, contributing to a deeper understanding of uncertainty in CT-based analyses and NN.**

***Keywords*—Microplastic, tomography, neural network**

I. Introduction

Microplastic (MPs) pollution has emerged as a significant environmental concern, with profound implications for marine ecosystems and human health [1]. These tiny plastic particles,lower than 5 mm and often invisible to the naked eye, can infiltrate aquatic environments, posing threats to marine life and potentially entering the food chain. Conventional methods for detecting MPs in marine organisms often involve invasive and time-consuming procedures, compromising sample integrity and yielding incomplete results with high possibility of sample contamination [2] [3] [4]. Consequently, there is a growing need for non-destructive and efficient methodologies that can accurately identify MPs in biological samples [5] [6]. In response to this challenge, we have developed an innovative methodology for detecting MPs in fish samples using computed tomography (CT) and neural network (NN). However, accurately assessing the uncertainty associated with these techniques is crucial.

In recent years significant efforts have been to address the challenges associated with uncertainty analysis in CT. Steiner et al. [7] provided a comprehensive analysis of tomography uncertainty, highlighting the importance of standards such as VDI/VDE 2617 and VDI/VDE 2630 in guiding the application of dimensional measurement techniques. Mueller et al. [8] presented a method for estimating measurement uncertainties in X-ray CT metrology using calibrated workpieces. Kiekens et al. [9] proposed a method for determining the uncertainty of dimensional measurements with industrial CT machines based on ISO-GUM principles. Additionally, Bredemann et al. [10] developed a method for task-specific uncertainty estimation in CT, while Jimenez et al. [11] presented a method for measurement uncertainty assessment of 3D complex geometries using micro-CT systems. Ferrucci et al. [12] utilized a Monte Carlo reconstruction technique to propagate uncertainty in x-ray CT. Furthermore, Antoran et al. [13] proposed a method to estimate uncertainty associated with CT using deep learning techniques, focusing on CT reconstruction rather than 3D object recognition.

In this paper, we build on these advances in uncertainty analysis and apply them to our new methodology, specifically on tomography-based imaging and NN, for the detection of MPs in fish samples and aim to improve the reliability and accuracy of our novel approach.

II. Material and methods

A. Sample preparation

Two experiments were conducted to analyze the presence and types of MPs in fish samples. Each experiment utilized two specimens of codfish (*Merluccius merluccius*), measuring 220 mm and 250 mm in length and weighing 87.3 g and 92.5 g, respectively. From each specimen, a truncated cone-shaped

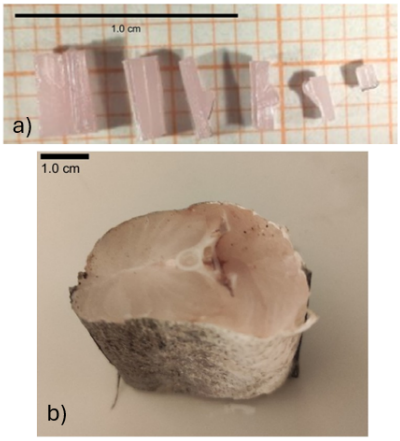

Fig. 1. Experiment 1. a) HDPE-2 microplastic samples of various sizes; b) Truncated cone-shaped fish sample microplastics

sample measuring 50 x 40 mm and weighing 21.5 g was extracted, encompassing all anatomical components, including skin, muscle, and bones.

In the first experiment, fish sample was prepared by embedding 11 pieces of the same type of polymer, namely HDPE-2. The MPs were selected to have a density range between 0.930 and 0.970 g/cm^3. Various shapes and sizes of HDPE-2 MPs were utilized, including cubic and parallelepiped forms, with dimensions ranging from 1x1x1 mm to 2.5x4x1 mm (Fig. 1).

In the second experiment, a targeted approach was adopted to evaluate both the distribution and types of MPs present in the fish samples. For density analysis purposes, two materials with high and low densities were strategically positioned at the beginning (1st layer) and end (5th layer) of the fish section, aiding in establishing a density range.

Precise cuts were made at varying heights within the fish to associate specific types of plastic with each layer. Each section received eight plastic inserts, including whole spheres, half spheres, quarter spheres, and eighth spheres, aiming to enable the identification of plastics with differing dimensions within the fish tissue.

Furthermore, to ensure accurate correspondence of plastic spheres in the tomographic images, small pieces of HDPE were inserted alongside the fish sample in each layer (Fig. 2).

The plastic types utilized in this experiment varied in composition and density, reflecting the diversity of plastics found in marine environments (Table I).

TABLE I. Summary of the different materials used, along with their corresponding densities.

Material	**Density [g/cm^3]**	**Layer**
ALUMINUM	2.51	1
NYLON FG 101L DUPONT (PA66)	1.14	2
POM ULTRAFORM H2320	1.41	3
TEFLON DF - 102	2.14	4
POLYSTYRENE	0.06	5

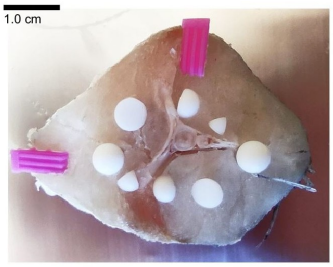

Fig. 2. Experiment 2: Truncated cone-shaped fish sample with eight white plastic inserts, including whole spheres, half spheres, quarter spheres eighth spheres and two pieces of pink HDPE

Both sets of experiments were designed to simulate realistic scenarios of MPs ingestion by marine organisms and to provide insights into the potential impacts of MPs pollution on marine ecosystems. To preserve the samples' original shape and prevent dehydration or deformation during CT scanning, a preservation technique involving immersion in a solution of agar-agar gel was employed. The gel, prepared by combining a 10% solution of agar-agar powder and water, was heated to 90°C until complete dissolution of the powder was achieved.

B. Tomograph set-up and CT image elaboration

The experimental setup relied on X-ray CT for visualizing and quantifying the internal density distribution of the samples using X-ray radiation [14] [15] [16]. A Zeiss Metrotom 1500 [17] system was utilized, offering a maximum measurement volume of 350 mm in the x, y, and z directions.

The acquisition duration for each scan was approximately two hours, setting an image averaging parameter to 3. In the first experiment, the resulting data had a specified spatial resolution of 40.31 µm, providing a complete volume of 1641x1242x1612 voxels. Meanwhile, in the second experiment, the spatial resolution was 36.34 µm, with a volume of 1641x1642x1642 voxels.

X-ray tomography generates a 16-bit 3D matrix where each voxel represents the local X-ray transparency of the material, corresponding to its density. However, visualizing such voluminous 3D datasets poses significant challenges due to their huge size, often comprising billions of values, and the inherent complexity of processing 3D information.

The conventional method involves presenting volumetric data as slices, as if crossing the object perpendicular to the slice. However, this approach introduces difficulties when implementing automated procedures, particularly for NN analysis of tomographic data.

Therefore, a choice was made to perform training and recognition directly on individual slices. Additionally, slices were extracted along all three axes - x, y, and z - to enhance the dataset's richness and analysis robustness.

C. Neural network

MPs detection in tomographic images from a prior experiment is achieved through binary semantic segmentation, a deep learning technique widely used for classifying and

locating objects in images [18]. The model takes as input the tomographic image, and outputs a binary mask, identifying MPs areas. The chosen architecture is based on DeepLabV3+, a state-of-the-art model for image segmentation, capable of capturing a wide range of contextual information from input at different scales allowing to determine the size of MPs to be segmented. The model, like previous solutions of semantic segmentation architectures, allows for the possibility of using different encoders, which can be selected from a pool of Convolutional Neural Networks (CNNs) available in the literature [19]. The model was initially trained on a dataset of images similar to those used in the current experiments. This prior training enabled the model to learn the specific characteristics and patterns associated with MPs, such as their density and shape. Given the wide range of plastic densities, it's crucial to note that density alone (i.e., image grayscale value) is not sufficient for accurate material selection, as other objects may have similar densities. Therefore, training the Deep Learning model is necessary to automatically identify specific tomographic features, such as density and shape, that were manually selected in the training dataset. This process is based on the known locations of MPs, resulting in a distinct grayscale pattern in the tomographic slices where MPs are present. The dataset, consisting of about 3000 CT images, was divided into training, validation and test sets. Specifically 2456 frames were used for training, 307 frames for validation, and 309 frames for testing. These frames are manually segmented, through a Python-based graphical user interface, in order to identify areas within the frames that show plastic residuals. Then, each processed frame will correspond to a binary mask, implementing a script written in Python and openCV. In order to increase the training dataset, diverse data augmentation techniques are applied, including random flipping (both horizontal and vertical), shifting, rotation, Gaussian noise, and perspective transformations. The hyper-parameters used for model training are optimized by implementing Bayesian optimization techniques, a method that has demonstrated superior performance over traditional methods like random search or grid search [20], [21]. To evaluate the segmentation ability of the model, the Jaccard index (also known as Intersection over Union, IoU) is chosen as the loss function. This index measures the ratio of overlap between the model's predicted segmentation and the actual ground truth. An early stop criterion is implemented during training, halting the process if there is no improvement in the validation loss for 5 consecutive epochs, with a maximum of 1000 epochs. The optimization aimed to maximize the IoU by systematically adjusting various input parameters, including batch size, optimizer, and learning rate. The Bayesian Optimization library for Python was used to manage the hyperparameter optimization process, facilitating intelligent exploration of the parameter space and iterative refinement of model hyperparameters to enhance performance. In both current experiments, the goal is to identify the locations of MPs with varying densities. The previously trained model is utilized to accurately detect and segment MPs in the tomographic images, leveraging its ability to discern subtle differences in density and shape that were learned during the training phase.

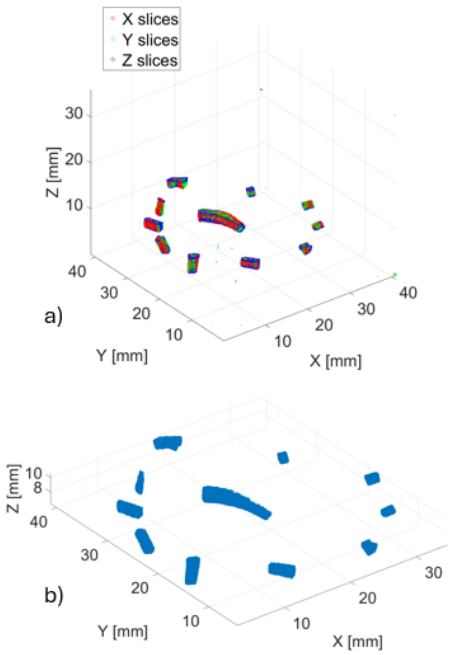

Fig. 3. Plot of the voxels recognized as plastic in x, y and z slices. a) Before post-processing b) after post-processing

.

III. Data post processing

Following the analysis phase, the obtained tomographic data underwent post-processing to refine the identification of plastic inclusions within the samples. This stage involved several steps aimed at enhancing the accuracy of the results while addressing potential sources of uncertainty. The main outcome is the generation of a map indicating the voxels where plastic inclusions have been detected. During the application of the NN model, a significant presence of false positives was observed, representing voxels where the network erroneously identifies plastic inclusions not actually present in the sample (Fig. 3.a). These false positives, often appearing as small-sized artifacts, can be mitigated through filtering techniques. However, such filtering compromises the resolution of the technique, making it challenging to distinguish between noise and accurately detected plastic. Further analysis involves the overlay of inferences obtained from slices oriented along the x, y, and z directions (Fig. 3.b). Remarkably, voxels representing plastic inclusions exhibit consistent characteristics across all directions, while false positives exhibit discrepancies.

To mitigate noise and enhance map accuracy, a criterion is applied wherein only voxels identified as plastic by all three inference directions are considered valid. This approach employs a logical "AND" operation among the three maps, eliminating voxels unrecognized as plastic by any single inference.

IV. Uncertainty analysis

In the proposed procedure, uncertainty can be classifiend based on its origin, the measured parameter, and its effect and type. In particular, we can distinguish:

- origin: in the acquisition stage in the tomographic system, in the processing stage by NN and in effect of post-processing;
- measured parameter: particle position, particle size, material (type of plastic);
- effect of uncertainty: false positives and false negatives, inaccurate data;
- type of uncertainty: epistemic, stochastic.

A. Uncertainty source

In the present work, uncertainty arises from three main sources: tomographic imaging, processing through NNs, and data post-processing. The tomographic imaging process inherently introduces uncertainty due to several factors, including resolution limitations, noise, and calibration issues. The use of NNs for post-processing tasks also introduces additional uncertainty into the analysis pipeline caused by model complexity, training data quality, and algorithmic variability. Lastly, data post-processing adds another source of uncertainty to the analysis process. This may include filtering errors, segmentation errors, and other possible distortions introduced during data manipulation. Managing these uncertainties is crucial for obtaining reliable and accurate results from the proposed methodology. Furthermore, taking inspiration from the approach used in 2D Blob Analysis [22], by considering image regions that contrast with the background, it is possible to extract detailed information on particle shape, size, and other characteristics, taking consideration the uncertainty issue. The threshold selection plays a crucial role in the process, directly influencing the particles identified and included in the final analysis.

B. Effect of uncertainty

Accuracy in identifying MPs is crucial to ensure the reliability of the results. However, during the analysis process, two types of errors may arise: false positives and false negatives [23]. False positives occur when the NN erroneously identifies regions without MPs as containing them. This can be due to artifacts from the tomograph, air inclusions, or other organic substances misclassified as MPs. Furthermore, the presence of MPs with characteristics similar to those of biological tissues, such as density or shape, can further complicate accurate detection. Strategies to mitigate false positives include implementing post-processing data filtering techniques. These techniques aim to remove regions incorrectly identified as MPs while balancing sensitivity with resolution preservation. Additional classification criteria based on size or material type can also help reject false positives during post-processing. Conversely, false negatives happen when the model fails to detect MPs present in the sample. This can happen due to variations in the shape, density, or distribution of MPs, which may make their correct identification by the model challenging. To reduce false negatives, it is crucial to optimize the model training phase. This may include increasing the complexity of the training dataset, using data augmentation techniques to expand the variability of training samples, and optimizing model parameters to improve its sensitivity in detecting MPs. During post-processing, adjusting threshold criteria can enhance sensitivity to MP detection, potentially increasing false positives. However, this approach can be beneficial for identifying all MPs present in samples, followed by a qualitative analysis to eliminate false positives.

C. Type of uncertainty

Like in the case of conventional sensors, in the context of data processing through deep learning, two main types of uncertainty emerge [24]: Epistemic Uncertainty arises from limitations in the available training data and knowledge, impeding the model's ability to acquire a comprehensive understanding. Insufficient data availability directly impacts the model's capacity to develop robust insights and predictions. Stochastic Uncertainty stems from the inherent randomness present in observations. Despite efforts to increase data volume, stochastic uncertainty persists, albeit improvements can be made to enhance data quality and environmental conditions. The established methodology relies on metrological tomography, ensuring a comprehensive understanding of machine parameters, including voxel resolution. However, even in machines with superior three-dimensional reconstruction capabilities, the presence of noise introduces stochastic uncertainty, affecting image contrast and quality. Consequently, this variability may hinder the network's efficacy in identifying inclusions. Notably, high epistemic uncertainty arises in scenarios with limited or absent training observations. For instance, if training exclusively involves specific shapes or sizes of inclusions, the network may struggle to recognize variations in geometries.

V. Results

A. Experiment 1

A single CT image containing MPs from the first experiment was used as reference for NN test under different level of contrast and noise. Contrast thresholds ranging from 0 to 1.9 were applied to the image, resulting in 255 distinct versions of the image. These images were processed by the NN to identify regions containing MPs. The results of the analysis are illustrated in Fig. 4.a

At the lowest contrast level, the NN erroneously identified the entire image as plastic (Fig 5.a). As the contrast level increased, the network's ability to discern non-plastic areas improved (Fig 5.b). At an intermediate level of contrast, the network reached a point where it failed to recognize any MPs within the image(Fig 5.c). Beyond this threshold, the network began accurately identifying plastic inclusions (Fig 5.d). This behavior underscores the importance of selecting an appropriate contrast level for optimal MPs detection.

Furthermore, random noise matrices were applied to the same CT image containing MPs. The noise levels were incrementally increased, and the resulting noisy images were

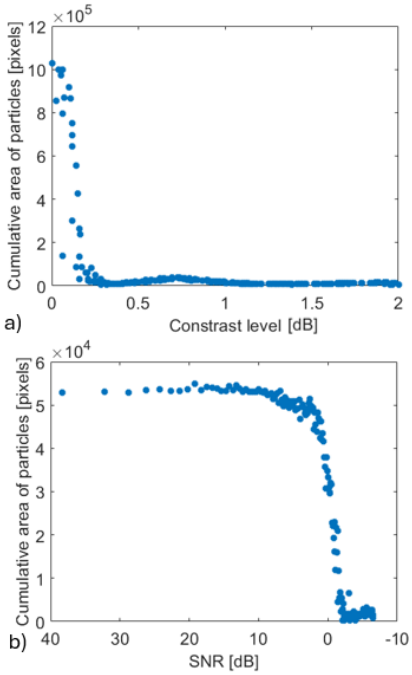

Fig. 4. Number of pixels identified as plastic across various a) contrast levels b)noise levels

processed by the NN to identify plastic regions. The results are illustrated in Fig. 6. At low noise levels, the NN successfully identified MP regions, with a deviation standard higher in the edge of the plastics 6.a. However, as the noise level increased, the accuracy of the network deteriorated, failing to identify the MPs correctly 6.b.

The graph in Fig. 4.b depicts the number of pixels identified as plastic at different noise levels. The results show an decreasing trend of number of pixels identified by the NN emphasizing the impact of noise on the accuracy of MPs detection.

B. Experiment 2

In the experiment 2, once the MPs were identified, they were classified based on the material by analyzing their X-ray

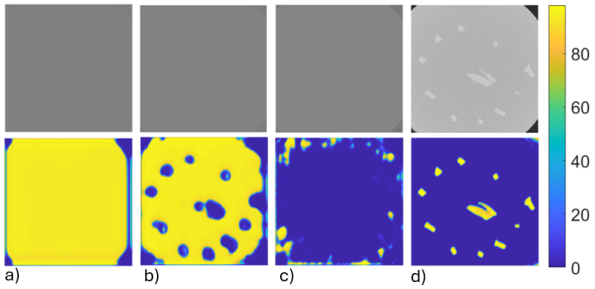

Fig. 5. Effect of contrast on microplastic detection. Top: CT images with different contrast levels. Bottom: Corresponding masks showing in yellow identified microplastic regions. a) 0.04 contrast level; b) 0.11 contrast level; c) 0.18 contrast level; d) 1.9 contrast level.

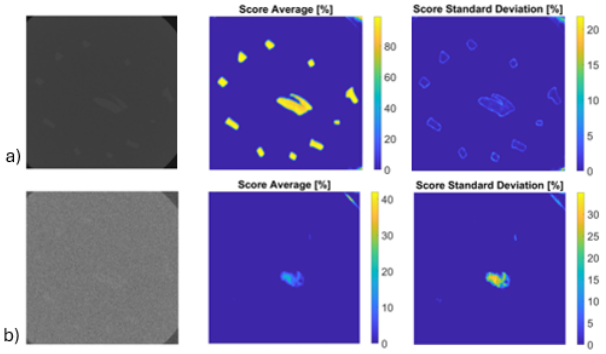

Fig. 6. Effect of noise on microplastic detection. First image: Noisy CT image. Second image: Corresponding masks showing score average from NN. Third image: Corresponding masks showing score standard deviation from NN. a) 30 dB signal-to-noise ratio; b) -3 dB signal-to-noise ratio.

transparency. To perform this evaluation, a system calibration was conducted (Fig. 7), as described in the "Sample Preparation" section of Experiment 2. Plastics may exhibit variability in their gray levels due to the presence of noise within the tomographic images. Therefore, regions of interest (RoI) were identified around the detected MPs, and the mean and standard deviation of the gray levels within the RoI were calculated. The calibration curve obtained by processing the tomographic images shows good linearity, with a standard deviation of $0.029 kg/m^3$.

VI. Discussion

Throughout our research, critical issues regarding the methodology for MPs detection in fish samples have been examined, focusing particularly on the intrinsic uncertainties arising from both the acquisition of images and their processing using NN and emphasizing the crucial importance of system calibration, data quality, and the application of appropriate thresholds.

The introduction of an adaptive threshold for the model emerges as a promising solution, facilitating more flexible uncertainty management and improving precision in determining particle volumes. Furthermore, notable generalization

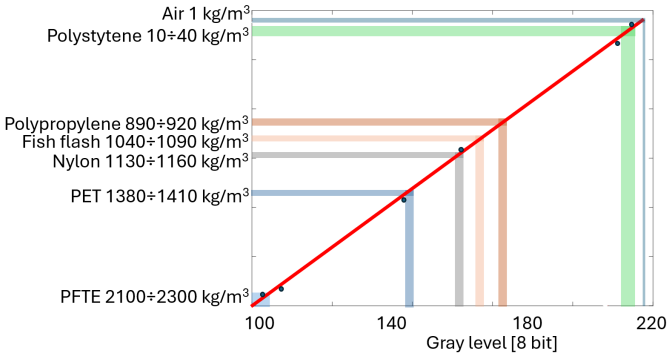

Fig. 7. Calibration gray

capability of NN has been observed, even in the presence of noisy images, suggesting that noise might inadvertently contribute to enhancing the model's generalization ability.

Another critical challenge concerns managing the uncertainty associated with the volume of individual particles, primarily assessed through their perimeter. However, it has been identified that using the AND algorithm to combine information from various imaging directions might compromise the accuracy of volume estimation. This underscores the importance of conducting thorough analysis on the implications of post-processing techniques on the overall accuracy of the methodology.

These considerations highlight the complexities and multifaceted aspects involved in adopting such a technique, emphasizing the necessity of rigorous evaluation and competent management of uncertainties.

VII. Conclusion

In summary, our proposed non-destructive method, combining CT scanning and NN processing, has yielded promising results in detecting MPs in fish samples. By leveraging recent advancements in uncertainty analysis, we've successfully identified and mitigated several sources of uncertainty from both imaging and NN processing, resulting in high accuracy and reliability. The present work uderscores the importance of system calibration, data quality, and the application of adaptive thresholds in enhancing detection accuracy. The generalization capability of the NN, even in noisy conditions, further demonstrates the robustness of out approach. Future research directions include further validation of the methodology across diverse sample types and environments. Additionally, integrating more advanced uncertainty quantification techniques could further enhance the reliability and robustness of the detection process. Overall, our work provides a solid foundation for the non-destructive detection of microplastics, offering a reliable tool for environmental monitoring and assessment of marine pollution.

References

[1] S. Sharma and S. Chatterjee, "Microplastic pollution, a threat to marine ecosystem and human health: A short review," Environmental Science and Pollution Research, vol. 24, no. 27, pp. 21 530–21 547, Aug. 2017, ISSN: 1614-7499. DOI: 10.1007/s11356-017-9910-8.

[2] W. Dellisanti, M. M. Leung, K. W. Lam, Y. Wang, M. Hu, H. S. Lo, J. K. H. Fang, "A short review on the recent method development for extraction and identification of microplastics in mussels and fish, two major groups of seafood," Marine Pollution Bulletin, vol. 186, pp. 114221, 2023, ISSN: 0025-326X. DOI: https://doi.org/10.1016/j.marpolbul.2022.114221.

[3] Q. Qiu, Z. Tan, J. Wang, J. Peng, M. Li, Z. Zhan, "Extraction, enumeration and identification methods for monitoring microplastics in the environment," Estuarine, Coastal and Shelf Science, vol. 176, pp. 102-109, 2016. DOI: 10.1016/j.ecss.2016.04.012.

[4] W. J. Shim, S. H. Hong, S. Eo, "Identification methods in microplastic analysis: A review," Analytical Methods, vol. 9, no. 9, pp. 1384-1391, 2017. DOI: 10.1039/c6ay02558g.

[5] M. M. Trusler, C. J. Sturrock, C. H. Vane, S. Cook, B. H. Lomax, "X-ray computed tomography: A novel non-invasive approach for the detection of microplastics in sediments," Marine Pollution Bulletin , vol. 194 pp. 115350, 2023, ISSN: 0025-326X. DOI: https://doi.org/10.1016/j.marpolbul.2023.115350.

[6] C. Tötzke, S. E. Oswald, A. Hilger, N. Kardjilov, "Non-invasive detection and localization of microplastic particles in a sandy sediment by complementary neutron and X-ray tomography," Journal of Soils and Sediments, vol. 21, no. 3, pp. 1476-1487, Mar. 2021, ISSN: 1614-7480. DOI: https://doi.org/10.1007/s11368-021-02882-6.

[7] D. Steiner, "Understanding accuracy for computed tomography," Quality magazine, 2024.

[8] P. Muller, J. Hiller, Y. Dai, J. Andreasen, H. Hansen, and L. De Chiffre, "Estimation of measurement uncertainties in x-ray computed tomography metrology using the substitution method," CIRP Journal of Manufacturing Science and Technology, vol. 7, no. 3, pp. 222–232, 2014, ISSN: 1755-5817. DOI: 10.1016/j.cirpj.2014.04.002.

[9] K. Kiekens, T. Ye, F. Welkenhuyzen, J.-P. Kruth, and W. Dewulf, "Uncertainty determination for dimensional measurements with computed tomography," 4th Conference on Industrial Computed Tomography (iCT), 2012.

[10] J. Bredemann and R. H. Schmitt, "Task-specific uncertainty estimation for medical ct measurements," Journal of Sensors and Sensor Systems, vol. 7, no. 2, pp. 627– 635, Dec. 2018, ISSN: 2194-878X. DOI: 10.5194/jsss-7-627-2018.

[11] R. Jimenez, M. Torralba, J. Yague-Fabra, S. Ontiveros, and G. Tosello, "Experimental approach for the uncertainty assessment of 3d complex geometry dimensional measurements using computed tomography at the mm and sub-mm scales," Sensors, vol. 17, no. 5, p. 1137, May 2017, ISSN: 1424-8220. DOI: 10.3390/s17051137.

[12] M. Ferrucci, E. Ametova, and W. Dewulf, "Monte carlo reconstruction: A concept for propagating uncertainty in computed tomography," Measurement Science and Technology, vol. 32, no. 11, p. 115 006, Jul. 2021, ISSN: 1361-6501. DOI: 10.1088/1361-6501/ac07db.

[13] J. Antoran, R. Barbano, J. Leuschner, J. M. Hernandez-Lobato, and B. Jin, "Uncertainty estimation for computed tomography with a linearised deep imageprior," Transactions on Machine Learning Research, 2023, ISSN: 2835-8856.

[14] Ente Nazionale Italiano di Unificazione, Non-destructive testing - industrial computed radiography with storage phosphor imaging plates - part 2: General principles for testing of metallic materials using x-rays and gamma rays, 2017. DOI: https : //www.iso.org/standard/67690.html.

[15] J. Kruth, M. Bartscher, S. Carmignato, R. Schmitt, L. De Chiffre, and A. Weckenmann, "Computed tomography for dimensional metrology," CIRP Annals, vol. 60, no. 2, pp. 821–842, 2011, ISSN: 0007-8506. DOI: 10.1016/j.cirp.2011.05.006.

[16] L. De Chiffre, S. Carmignato, J.-P. Kruth, R. Schmitt, and A. Weckenmann, "Industrial applications of computed tomography," CIRP Annals, vol. 63, no. 2, pp. 655–677, 2014, ISSN: 0007-8506. DOI: 10 . 1016 / j.cirp.2014.05.011.

[17] Carl Zeiss Unternehmensbereich Ind. Messtechnik GmbH, Metrotom os user software for ct scanners, Carl Zeiss Unternehmensbereich Ind. Messtechnik GmbH, D-73446 Oberkochen, 201.

[18] N. Giulietti, A. Caputo, P. Chiariotti, and P. Castellini, "Swimmernet: Underwater 2d swimmer pose estimation exploiting fully convolutional neural networks," Sensors, vol. 23, no. 4, p. 2364, 2023.

[19] L.-C. Chen, Y. Zhu, G. Papandreou, F. Schroff, and H. Adam, "Encoder-decoder with atrous separable convolution for semantic image segmentation," in Proceedings of the European conference on computer vision (ECCV), 2018, pp. 801–818.

[20] N. Giulietti, S. Discepolo, P. Castellini, and M. Martarelli, "Correction of substrate spectral distortion in hyper-spectral imaging by neural network for blood stain characterization," Sensors, vol. 22, no. 19, p. 7311, 2022.

[21] N. Giulietti, S. Discepolo, P. Castellini, and M. Martarelli, "Neural network based hyperspectral imaging for substrate independent bloodstain age estimation," Forensic Science International, vol. 349, p. 111 742, 2023.

[22] F. Parzer, C. Kirisits, and O. Scherzer, "Uncertainty quantification for scale-space blob detection," arXiv preprint arXiv:2307.15489, 2023.

[23] G. L. F. d. Silva, T. L. A. Valente, A. C. Silva, A. C. de Paiva, and M. Gattass, "Convolutional neural network-based pso for lung nodule false positive reduction on ct images," Computer Methods and Programs in Biomedicine, vol. 200, p. 105 924, 2021.

[24] M. Kana, "Uncertainty in deep learning. how to measure?" Towarddatascience.com, Apr. 2020.